Science of the Total Environment 913 (2024) 169692

Contents lists available at ScienceDirect

Science of the Total Environment

journal homepage: www.elsevier.com/locate/scitotenv

Incorporating high-resolution climate, remote sensing and topographic data to map annual forest growth in central and eastern Europe

Jernej Jevšenak [a,b,*], Marcin Klisz [c], Jiří Mašek [d], Vojtěch Čada [e], Pavel Janda [e], Miroslav Svoboda [e], Ondřej Vostarek [e], Vaclav Treml [d], Ernst van der Maaten [f], Andrei Popa [g,h], Ionel Popa [g], Marieke van der Maaten-Theunissen [f], Tzvetan Zlatanov [i], Tobias Scharnweber [j], Svenja Ahlgrimm [j], Juliane Stolz [f,k], Irena Sochová [l,m], Cătălin-Constantin Roibu [n], Hans Pretzsch [a], Gerhard Schmied [a], Enno Uhl [a,o], Ryszard Kaczka [d], Piotr Wrzesiński [c], Martin Šenfeldr [p], Marcin Jakubowski [q], Jan Tumajer [d], Martin Wilmking [j], Nikolaus Obojes [r], Michal Rybníček [l,m], Mathieu Lévesque [s], Aleksei Potapov [t], Soham Basu [u], Marko Stojanović [m], Stefan Stjepanović [v], Adomas Vitas [w], Domen Arnič [x], Sandra Metslaid [t], Anna Neycken [s], Peter Prislan [x], Claudia Hartl [y,z], Daniel Ziche [aa], Petr Horáček [l,m], Jan Krejza [u,m], Sergei Mikhailov [l,m], Jan Světlík [u,m], Aleksandra Kalisty [ab], Tomáš Kolář [l,m], Vasyl Lavnyy [ac], Maris Hordo [t], Walter Oberhuber [ad], Tom Levanič [ae,af], Ilona Mészáros [ag], Lea Schneider [ah], Jiří Lehejček [ai], Rohan Shetti [ai], Michal Bošeľa [aj], Paul Copini [ak,al], Marcin Koprowski [am,an], Ute Sass-Klaassen [ak,ao], Şule Ceyda Izmir [ap], Remigijus Bakys [aq], Hannes Entner [ad], Jan Esper [ar], Karolina Janecka [j,as], Edurne Martinez del Castillo [ar], Rita Verbylaite [at], Mátyás Árvai [au], Justine Charlet de Sauvage [s], Katarina Čufar [av], Markus Finner [ad], Torben Hilmers [a], Zoltán Kern [aw,ax], Klemen Novak [av], Radenko Ponjarac [ay], Radosław Puchałka [am,an], Bernhard Schuldt [az], Nina Škrk Dolar [av], Vladimir Tanovski [ba], Christian Zang [bb,a], Anja Žmegač [bb,a], Cornell Kuithan [f], Marek Metslaid [bc], Eric Thurm [k], Polona Hafner [ae], Luka Krajnc [ae], Mauro Bernabei [bd], Stefan Bojić [v], Robert Brus [be], Andreas Burger [j], Ettore D'Andrea [bf,bg], Todor Đorem [v], Mariusz Gławęda [bh], Jožica Gričar [bi], Marko Gutalj [v], Emil Horváth [bj], Saša Kostić [ay], Bratislav Matović [ay,v], Maks Merela [av], Boban Miletić [v], András Morgós [bk], Rafał Paluch [bl], Kamil Pilch [bl], Negar Rezaie [bf], Julia Rieder [az], Niels Schwab [bm], Piotr Sewerniak [bn], Dejan Stojanović [ay], Tobias Ullmann [bo], Nella Waszak [an], Ewa Zin [bl,bp], Mitja Skudnik [b,be], Krištof Oštir [bq], Anja Rammig [a], Allan Buras [a]

[a] *TUM School of Life Sciences, Technical University of Munich, Germany*
[b] *Department for Forest and Landscape Planning and Monitoring, Slovenian Forestry Institute, Slovenia*
[c] *Dendrolab IBL, Department of Silviculture and Forest Tree Genetics, Forest Research Institute, Poland*
[d] *Department of Physical Geography and Geoecology, Faculty of Science, Charles University, Czech Republic*
[e] *Faculty of Forestry and Wood Sciences, Czech University of Life Sciences Prague, Czech Republic*
[f] *Chair of Forest Growth and Woody Biomass Production, TU Dresden, Germany*
[g] *National Institute for Research and Development in Forestry "Marin Drăcea", Romania*
[h] *Faculty of Silviculture and Forest Engineering, Transilvania University of Brasov, Romania*
[i] *Institute of Biodiversity and Ecosystem Research, Bulgarian Academy of Sciences, Bulgaria*
[j] *DendroGreif, Institute of Botany and Landscape Ecology, Greifswald University, Germany*
[k] *Department of Forest Planning/Forest Research/Information Systems, Research Unit Silviculture and Forest Growth, Landesforst Mecklenburg-Vorpommern, Germany*
[l] *Department of Wood Science and Wood Technology, Mendel University in Brno, Czech Republic*
[m] *Global Change Research Institute of the Czech Academy of Sciences, Czech Republic*
[n] *Forest Biometrics Laboratory, Faculty of Forestry, "Stefan cel Mare" University of Suceava, Romania*

* Corresponding author at: TUM School of Life Sciences, Technical University of Munich, Germany.
E-mail address: jernej.jevsenak@gozdis.si (J. Jevšenak).

https://doi.org/10.1016/j.scitotenv.2023.169692
Received 20 October 2023; Received in revised form 12 December 2023; Accepted 24 December 2023
Available online 29 December 2023

[o] Bavarian State Institute of Forestry, Germany
[p] Department of Forest Botany, Dendrology and Geobiocoenology, Mendel University in Brno, Czech Republic
[q] Department of Forest Utilisation, Faculty of Forest and Wood Technology, Poznań University of Life Sciences, Poland
[r] Institute for Alpine Environment, Eurac Research, Italy
[s] Silviculture Group, Institute of Terrestrial Ecosystems, ETH Zurich, Switzerland
[t] Chair of Forest and Land Management and Wood Processing Technologies, Estonian University of Life Sciences, Estonia
[u] Department of Forest Ecology, Mendel University in Brno, Czech Republic
[v] Department of Forestry, Faculty of Agriculture, University of East Sarajevo, Bosnia and Herzegovina
[w] Vytautas Magnus University, Lithuania
[x] Department for Forest Technique and Economics, Slovenian Forestry Institute, Slovenia
[y] Nature Rings – Environmental Research and Education, Germany
[z] Panel on Planetary Thinking, Justus-Liebig-University, Germany
[aa] Faculty of Forest and Environment, Eberswalde University for Sustainable Development, Germany
[ab] Faculty of Forestry, Bialystok University of Technology, Poland
[ac] Department of Silviculture, Ukrainian National Forestry University, Ukraine
[ad] Department of Botany, University of Innsbruck, Austria
[ae] Department of Forest Yield and Silviculture, Slovenian Forestry Institute, Slovenia
[af] Faculty of Mathematics, Natural Sciences and Information Technologies, University of Primorska, Slovenia
[ag] Department of Botany, Faculty of Science and Technology, University of Debrecen, Hungary
[ah] Department of Geography, Justus-Liebig-University, Germany
[ai] Department of Environment, Faculty of Environment, Jan Evangelista Purkynė University, Czech Republic
[aj] Department of Forest Management Planning and Informatics, Faculty of Forestry, Technical University in Zvolen, Slovakia
[ak] Forest Ecology and Forest Management (FEM), Wageningen University & Research, the Netherlands
[al] Wageningen Environmental Research, Wageningen University & Research, the Netherlands
[am] Department of Ecology and Biogeography, Faculty of Biological and Veterinary Sciences, Nicolaus Copernicus University, Poland
[an] Centre for Climate Change Research, Nicolaus Copernicus University, Poland
[ao] van Hall Larenstein Applied University, the Netherlands
[ap] Department of Forest Botany, Faculty of Forestry, Istanbul University-Cerrahpaşa, Turkey
[aq] Department of Forestry, Kaunas Forestry and Environmental Engineering University of Applied Sciences, Lithuania
[ar] Department of Geography, Johannes Gutenberg University, Germany
[as] Climate Change Impacts and Risks in the Anthropocene (C-CIA), Institute for Environmental Sciences, University of Geneva, Switzerland
[at] Department of Forest Genetics and Tree Breeding, Lithuanian Research Centre for Agriculture and Forestry, Lithuania
[au] Institute for Soil Sciences, HUN-REN Centre for Agricultural Research, Hungary
[av] Department of Wood Science and Technology, Biotechnical Faculty, University of Ljubljana, Slovenia
[aw] Institute for Geological and Geochemical Research, HUN-REN Research Centre for Astronomy and Earth Sciences, Hungary
[ax] CSFK, MTA Centre of Excellence, Budapest, Hungary
[ay] Institute of Lowland Forestry and Environment, University of Novi Sad, Serbia
[az] Chair of Forest Botany, TU Dresden, Germany
[ba] Hans Em, Faculty of Forest Sciences, Landscape Architecture and Environmental Engineering, Ss. Cyril and Methodius, University in Skopje, North Macedonia
[bb] Department of Forestry, University of Applied Sciences Weihenstephan-Triesdorf, Germany
[bc] Institute of Forestry and Engineering, Estonian University of Life Sciences, Estonia
[bd] Institute of BioEconomy, National Research Council, Italy
[be] Department of Forestry and Renewable Forest Resources, Biotechnical Faculty, University of Ljubljana, Slovenia
[bf] Research Institute on Terrestrial Ecosystems (IRET), National Research Council of Italy (CNR), Italy
[bg] National Biodiversity Future Centre – NBFC, Italy
[bh] Stefan Żeromski High School No 2 with Bilingual Departments in Sieradz, Poland
[bi] Department of Forest Physiology and Genetics, Slovenian Forestry Institute, Slovenia
[bj] Independent researcher, Hungary
[bk] Consart Bt., Hungary
[bl] Dendrolab IBL, Department of Natural Forests, Forest Research Institute (IBL), Poland
[bm] Centre for Earth System Research and Sustainability (CEN), Institute of Geography, Universität Hamburg, Germany
[bn] Department of Soil Science and Landscape Management, Nicolaus Copernicus University, Poland
[bo] Department of Remote Sensing, Institute of Geography and Geology, University of Würzburg, Germany
[bp] Southern Swedish Forest Research Centre, Swedish University of Agricultural Sciences (SLU), Sweden
[bq] Faculty of Civil and Geodetic Engineering, University of Ljubljana, Slovenia

HIGHLIGHTS

- We combined remote sensing, climate and elevation to model tree-ring width (TRW).
- Models' explained variance ranged up to 52 % and was higher for species-specific models.
- Including remote sensing data improved the prediction accuracy by 6 % on average.
- Satellite-derived vegetation indices yielded strong positive relationships with TRW.
- The developed forest-type models were successfully applied to generate a map of TRW.

GRAPHICAL ABSTRACT

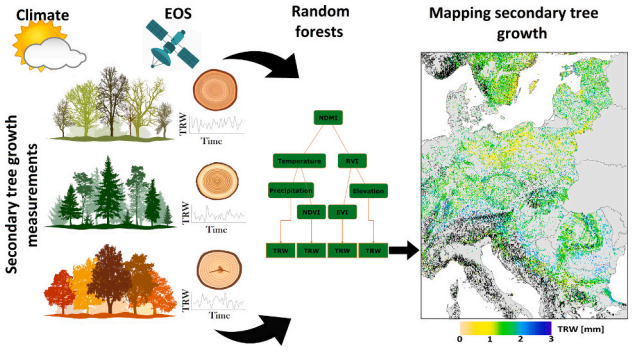

ARTICLE INFO

Editor: Elena Paoletti

Keywords:
Sentinel-1
Sentinel-2
Tree rings
NDMI
NDRE
Random forest

ABSTRACT

To enhance our understanding of forest carbon sequestration, climate change mitigation and drought impact on forest ecosystems, the availability of high-resolution annual forest growth maps based on tree-ring width (TRW) would provide a significant advancement to the field. Site-specific characteristics, which can be approximated by high-resolution Earth observation by satellites (EOS), emerge as crucial drivers of forest growth, influencing how climate translates into tree growth. EOS provides information on surface reflectance related to forest characteristics and thus can potentially improve the accuracy of forest growth models based on TRW. Through the modelling of TRW using EOS, climate and topography data, we showed that species-specific models can explain up to 52 % of model variance (*Quercus petraea*), while combining different species results in relatively poor model performance (R^2 = 13 %). The integration of EOS into models based solely on climate and elevation data improved the explained variance by 6 % on average. Leveraging these insights, we successfully generated a map of annual TRW for the year 2021. We employed the area of applicability (AOA) approach to delineate the range in which our models are deemed valid. The calculated AOA for the established forest-type models was 73 % of the study region, indicating robust spatial applicability. Notably, unreliable predictions predominantly occurred in the climate margins of our dataset. In conclusion, our large-scale assessment underscores the efficacy of combining climate, EOS and topographic data to develop robust models for mapping annual TRW. This research not only fills a critical void in the current understanding of forest growth dynamics but also highlights the potential of integrated data sources for comprehensive ecosystem assessments.

1. Introduction

Forest growth is considered of essential importance due to its climate-mitigation potential via carbon sequestration, its economic value in terms of providing renewable resources and its indirect contribution to other key ecosystem services. Across the globe, forest growth varies with biomes and climate, species composition and forest developmental stage and structure (Gough et al., 2019; Morreale et al., 2021), terrain characteristics, soil quality and nutrient availability (Coops and Waring, 2001). However, ongoing environmental changes pose potential risks to forests by amplifying drought stress and mortality rates, depositing nitrogen pollutants and increasing disturbances, such as fires, windstorms and insect outbreaks (Bugmann et al., 2014). All of these risks challenge forest management and therefore deserve further investigation in order to increase the climate resilience of forests (Keenan, 2015). Under this framework, observation-based gridded growth products can provide a valuable source of information, since they allow climate-change impacts on forest growth across large spatial gradients to be quantified. Despite recent advances in tree-growth modelling (Coops et al., 2021; Gallaun et al., 2010; Gang et al., 2017; Tian et al., 2023; Verkerk et al., 2015; Wu et al., 2023; Wulder et al., 2020), a critical gap persists in the availability of observation-based, high-resolution, empirical gridded products (maps) depicting forest growth. Unlike growth predictions derived from dynamic vegetation models (Quillet et al., 2010), the absence of such maps hinders our ability to obtain precise insights into the dynamics of forest ecosystems. These empirical maps, if developed, could serve a multitude of purposes and offer valuable large-scale quantitative information on forests' responses to climate change. Notably, they could facilitate the assessment of drought impacts on forest ecosystems, providing direct insights into carbon sequestration processes and enabling the evaluation of drought resilience in these vital ecological systems. The development and utilisation of such maps stand to significantly enhance our understanding of the intricate relationships between forests and their changing environments.

In this context, tree-ring width (TRW) data are an invaluable source of information, since they represent trees' aboveground secondary growth at annual resolution – and thus approximate changes in tree growth and net primary production (NPP) (Dye et al., 2016; Wang et al., 2023). However, TRW records represent local tree growth, which implies the necessity of upscaling TRW-based NPP estimates to the stand and landscape levels in order to achieve gridded products (Babst et al., 2018). In their study, Bodesheim et al. (2022) employed a series of climate variables to generate annual maps of secondary tree growth across various species. However, it is crucial to acknowledge that local site conditions, shaped by interacting soil and forest stand characteristics, play a pivotal role in modulating how climate factors contribute to secondary tree growth, underscoring the necessity of incorporating local context when mapping forest growth (Collalti et al., 2020; Dorado-Liñán et al., 2022; Rehschuh et al., 2017; Schmitt et al., 2020). Thus, high-resolution, site-specific information could improve empirical models for predicting TRW based on gridded climate data (Babst et al., 2018; Bodesheim et al., 2022).

Earth observation by satellites (EOS) provides a cost-effective and non-intrusive method for observing and monitoring large areas at a high resolution, thereby enabling comprehensive evaluations of vegetation dynamics. EOS may be a valuable and easy-to-obtain source of site-specific information by providing spectral data on the forest surface, which is closely related to photosynthetic activity and tree growth (Martínez-Fernández et al., 2019). Recent advancements in remote sensing technology now facilitate the monitoring of vegetation dynamics at high resolution, exemplified by platforms such as the Sentinel-1 and Sentinel-2 satellites, both of which were leveraged in our study, and allow for the integration of passive and active satellite sensors and thus a more sophisticated modelling of tree growth.

Passive multispectral sensors (optical EOS) are a well-explored means of approximating secondary tree growth by measuring canopy reflectance at different wavelengths, which ultimately allows reflectance to be expressed using various vegetation indices (Fu and Sun, 2022; Xue and Su, 2017). Previous studies have successfully linked secondary tree growth and vegetation indices on a global scale (Bhuyan et al., 2017; Vicente-Serrano et al., 2016), in boreal forests (Andreu-Hayles et al., 2011; Babst et al., 2018; Beck et al., 2013; Brehaut and Danby, 2018; Kaufmann et al., 2004) and at more local scales in temperate forests (Bonney and He, 2021; Correa-Díaz et al., 2019; Decuyper et al., 2020; Mašek et al., 2023; Mašek et al., 2024; Pompa-García et al., 2021; Stolz et al., 2021; Vicente-Serrano et al., 2020). Most studies applied EOS featuring coarse (e.g. GIMMS with 8 km) to moderate (e.g. MODIS with 250 m) resolutions and solely relied on the commonly used normalised difference vegetation index (NDVI). In contrast, our research utilised the high-resolution (10–20 m) Sentinel-2 data to calculate four distinct vegetation indices, a novel approach that has not yet been compared with tree-ring data. The NDVI is a measure of vegetation greenness and density that is directly related to photosynthetic activity and represents a suitable proxy for NPP. Other vegetation indices, such as the normalised difference moisture index (NDMI), the normalised difference red edge index (NDRE) and the enhanced vegetation index (EVI) require further exploration regarding their relations

to secondary tree growth. Similar to the NDVI, the EVI and NDRE increase with higher photosynthetic activity but incorporate different wavelengths. Finally, the NDMI reflects moisture content in vegetation, offering valuable insights into plant water status and thereby presenting significant potential for the precise estimation of tree growth.

In contrast to optical EOS, synthetic aperture radar (SAR) is a type of active satellite sensor and a less-explored source of EOS for studying forest growth. The radar vegetation index (RVI) is calculated from Sentinel-1 vertical–vertical (VV) and vertical–horizontal (VH) backscattering coefficients and is sensitive to surface roughness, geometrical properties of the vegetation, water content and leaf area index (Mandal et al., 2020; Tsyganskaya et al., 2018; Vreugdenhil et al., 2018). Since growth is linked to plant water availability (Castagneri et al., 2022; Dobbertin, 2005), SAR could improve models that explain variations in secondary tree growth (Knapp and Smith, 2001). Despite these possible indirect effects between SAR and tree growth, SAR data have not yet been linked to secondary tree growth. Incorporating the high-resolution (10–20 m) EOS sources with site-specific climate and topography data into observation-based tree-growth models appears to be a promising avenue for large-scale mapping of annual TRW.

In our study, we delineated three primary objectives: 1) Integrating climate variables, EOS and elevation data to develop models for predicting TRW on different levels: species-specific, forest type-specific and a general model using all data. To achieve this, we assembled TREOS – a sub-continental tree-ring and EOS network. 2) Quantifying the added value of incorporating EOS into climate-based predictions of TRW. Given the previously described links between EOS and tree growth, we hypothesised that EOS information significantly increases the prediction accuracy of TRW. 3) To upscale the established forest-type models to the afforested area within the study region and derive the spatial extent of reliable TRW predictions. This process aimed to underscore the practical applications and real-world relevance of the models we developed.

2. Materials and methods

2.1. The TREOS tree-ring network

We compiled a large tree-ring network of 707 site chronologies (Fig. 1). Chronologies come from eight abundant and five minor tree species from across central and eastern Europe and include 17,969 individual tree growth measurements over an elevational range of 8 to 1682 m asl. Across the sites, the growing season (April–September) mean temperature ranges from 6.9 °C to 19.7 °C, and the annual precipitation totals are between 450 mm and 2100 mm, thus covering a large range of climatic conditions. All the chronologies were sampled from 2018 onwards, ensuring a minimum overlap with the Sentinel-1 and Sentinel-2 data of two years per site. Tree-ring sampling was undertaken at the end of the growing season to ensure that the secondary growth of a given year was completed. The number of sites declined over time, with 30 site chronologies remaining in 2022 (Supplementary Fig. 7). The sampling protocol followed standardised criteria to minimise potential biases. First, the sampled tree species had to be dominant in the stand – that is, they should represent the canopy layer. Next, a minimum of 10 trees per site was required. The sampled species had to belong to one of the *Fagus*, *Picea*, *Pinus*, *Quercus*, *Abies* or *Pseudotsuga* genera to emphasise abundant and economically important forest trees in the study region. Some less representative tree species belonging to the same genera as the main species were included in the models that combined different tree species – that is, the forest-type and the general models. These additional tree species encompassed *Quercus* spp. (12 sites), *Quercus cerris* (9), *Pinus strobus* (5), *Fagus orientalis* (3), *Pinus peucea* (1) and *Pinus sitchensis* (1). We initiated a tree-ring network, whose members applied a consistent sampling design and provided eventual measurements of tree-ring widths (TRW). Measurements were obtained using standard dendrochronological methods, which include tree coring or stem disc collection, drying and surface preparation, followed by ring-width measurements from high resolution images (e.g. using CooRecorder) or specialised tree-ring measuring stages (e.g. LinTab) (Speer, 2010). Cross-dating was applied to ensure that each individual tree ring was assigned its exact year of formation (Wigley et al., 1987). Each site chronology is a time series of mean annual radial increment obtained by averaging TRWs from individual trees. That is, before averaging, we did not detrend individual TRW measurements to retain absolute values of secondary growth as the dependent variable, which is more meaningful in terms of representing secondary tree growth, since detrending methods would centre all values around a value of 1 and thus remove differences of absolute growth among the sites.

2.2. Earth observation by satellites (EOS)

Each site location was carefully verified to ensure that it was at least 100 m from the nearest forest edge. We extracted individual Sentinel-1 and Sentinel-2 bands for a circular polygon with a radius of 100 m around the coordinates of each sampling site using Google Earth Engine (Gorelick et al., 2017). The 100 m radius was selected since many sampling sites were located relatively close to the forest edge, and as the radius increases, the probability of capturing non-forest areas increases rapidly. For Sentinel-2, we extracted cloud-free, orthorectified, atmospherically corrected surface reflectance of all the required bands (Level-2A), which was available from March 2017. From the bands obtained, we computed the NDVI, EVI, NDRE and NDMI based on Eqs. (1) to (4), where NIR, SWIR, Red, Blue and VRE stand for near infrared (B8), shortwave infrared (B11), red (B4), blue (B2) and vegetation red edge (B8A) bands, respectively. In addressing potential non-forest cover, such as roads and forest gaps, we explored different percentages for removing pixels having the lowest NDVI values within each polygon. Simultaneously, we evaluated the explained variance in relation to the validation data, identifying optimal results with a removal threshold set at 7 %. Subsequently, we experimented with various percentiles for aggregating site- and time-step-specific vegetation indices into seasonal values. The highest model performance was achieved at the 75th percentile, the same value utilised in the models presented in this study. To further refine the data and mitigate potential artefacts, we applied masking to eliminate values below predetermined thresholds for each vegetation index. Specifically, thresholds of 0.25, 0.20, 0.10 and 0 were established for NDVI, EVI, NDRE and NDMI, respectively. This meticulous process resulted in the removal of an average of 1.54 % of the original data across all vegetation indices. These refinements contribute to the robustness and accuracy of our analysis by enhancing the quality of the input data and ensuring the reliability of subsequent model outcomes.

$$NDVI = (NIR - Red)/(NIR + Red) \quad (1)$$

$$EVI = 2.5 \cdot (NIR - Red)/(NIR + 6 \cdot Red - 7.5 \cdot Blue + 1) \quad (2)$$

$$NDMI = (NIR - SWIR)/(NIR + SWIR) \quad (3)$$

$$NDRE = (NIR - VRE)/(NRE + VRE) \quad (4)$$

Since 2014, the Sentinel-1 mission has provided data from a dual-polarisation C-band SAR instrument and offers the advantage of acquiring reliable data in all weather and lighting conditions. We used the Sentinel-1 ground range detected (GRD) data collection, processed with the Sentinel-1 Toolbox (Veci et al., 2014), to generate a calibrated, orthorectified product, which includes all the Sentinel 1-A and 1-B GRD image products acquired in both ascending and descending orbits. To reduce the unwanted artefacts or distortions that can occur at the edges or borders of the images, we applied additional border-noise correction, speckle filtering and radiometric terrain normalisation using the procedure proposed by Mullissa et al. (2021). We used the images acquired in the descending orbit, the interferometric wide swath (IW) mode and

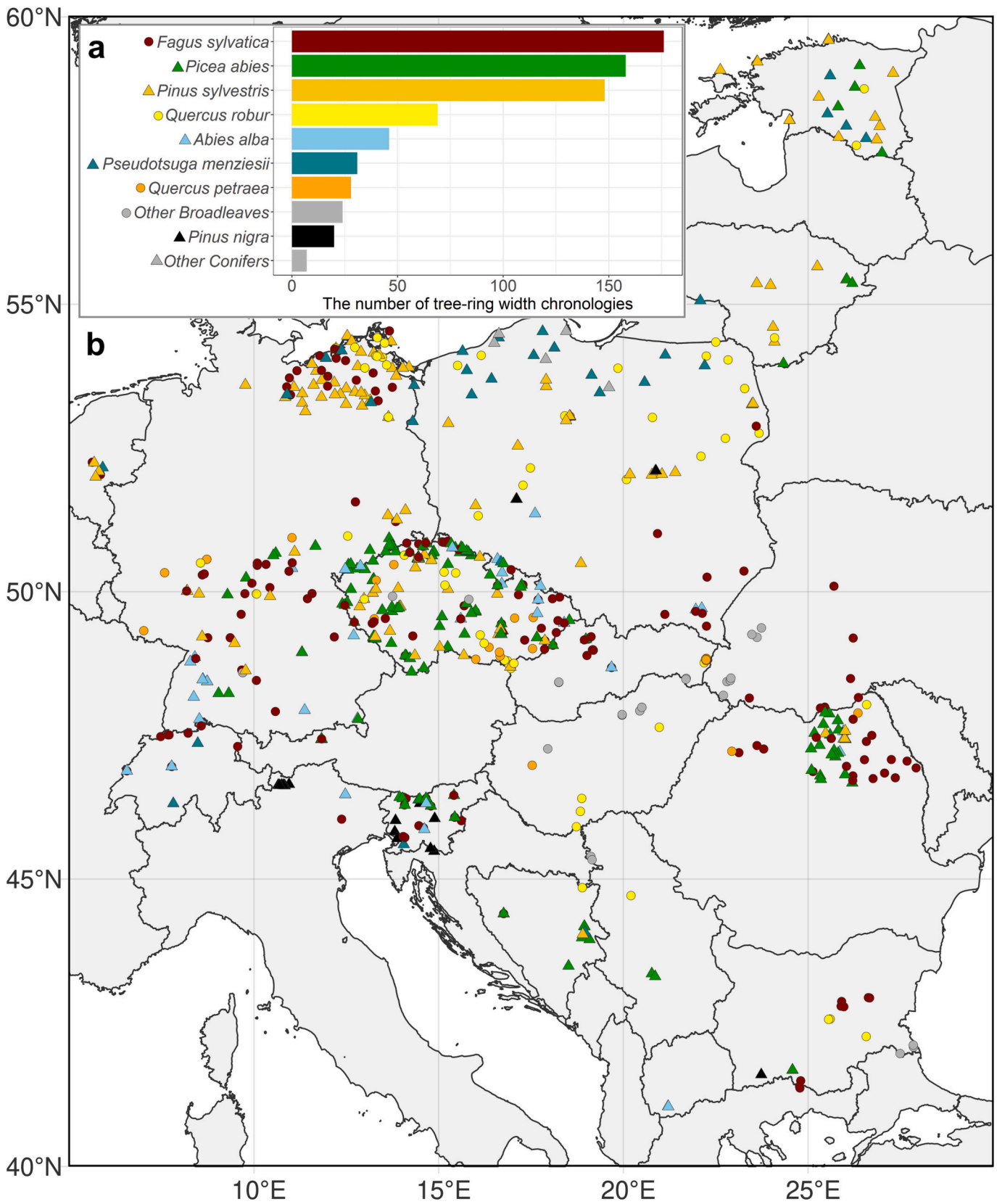

Fig. 1. TREOS network including 707 tree-ring width chronologies sampled in central and eastern Europe since 2018. The number of study sites of the main tree species included in the analyses (a) and their spatial distribution across the TREOS network (b).

the dual-polarisation state (VV/VH). Finally, we calculated the dual-polarimetric radar vegetation index (RVI) (Mandal et al., 2020) (Eq. (5)).

$$RVI = \sqrt{\frac{VV}{VV + VH}}\left(4VH\frac{VV}{VH}\right) \quad (5)$$

To derive a diverse set of potential EOS-based predictor variables, we averaged both Sentinel-2 vegetation indices and Sentinel-1 RVI, VV and VH polarisation bands into seasonal aggregates spanning from March to October. These aggregates were defined with a minimum length of two consecutive months (e.g. March–April) and a maximum of eight months (i.e. March–October). The resulting seasonal aggregates capture varying vegetation states throughout the year, which are probably crucial for modelling TRWs. In our approach, we excluded seasonal aggregates related to the previous growing season due to the limited number of overlapping years with Sentinel-2, although many studies have reported significant relationships between tree rings and the NDVI from previous growing seasons (Bhuyan et al., 2017; Correa-Díaz et al., 2019; Vicente-Serrano et al., 2016).

2.3. Climate and environmental model predictors

We extracted mean, minimum and maximum daily temperatures and precipitation sums for each site from the nearest grid point in the European daily high-resolution climate dataset (*E*-OBS v25.0e) at 0.1-degree resolution (Cornes et al., 2018). To account for the extreme drought effects on tree growth (Buras et al., 2020; Salomón et al., 2022), we considered the climatic water balance. First, the potential evapotranspiration (PET) was calculated using the Hargreaves equation (Hargreaves and Samani, 1982), and to obtain the climatic water balance, the PET was subtracted from the daily precipitation sum (Jevšenak, 2019). Similar to the EOS data, the climate data were aggregated into different seasonal combinations, ranging from March to October, with a minimum length of two months and a maximum of eight months. To account for the influence of the previous year's climate, which often exerts a significant impact on TRW in the current year, we also incorporated climate data from August to October of the preceding year. In addition, to capture the broader climatic context, the long-term (2000–2022) growing season (April–September) mean temperatures, annual climatic water balance and precipitation sums were calculated to accommodate diverse climates. All the climate variables were then considered as potential predictors in the modelling part. Next, each site was classified as coniferous, broadleaved or mixed forest according to the CORINE (Coordination of Information on the Environment) land cover classification representing forest cover in 2018 (Büttner, 2014). Site elevation was derived from the EU-DEM raster digital elevation model with 25 m resolution (https://land.copernicus.eu/imagery-in-situ/eu-dem).

In addition to the previously mentioned predictor variables, we explored additional factors derived from site-specific stand characteristics from the tree-ring data. Specifically, we investigated stand age and mean growth rates, which yielded a significant improvement in the model performance (not shown). However, since these variables are not available on a gridded scale – in contrast to the remaining predictor variables – and, thus, cannot be applied to upscale local tree growth, we did not include them in our final model selection.

2.4. Model design and validation

We modelled the associations between TRW as the dependent variable and a range of seasonal climate aggregates (including temperature, precipitation and water balance), as well as aggregated EOS variables (NDVI, NDRE, EVI, NDMI, RVI, VV and VH backscattering coefficients) along with elevation, serving as independent variables (Objective 1). To do so, we employed the random forest algorithm, which is an ensemble learning method that combines predictions from multiple decision trees to reduce the risk of overfitting and provide more accurate and robust predictions (Ho, 1995). In an exploratory phase, we tested several different algorithms, including artificial neural networks, multiple linear regressions with interactions and generalised additive models. Since random forests consistently provided the most accurate predictions in terms of the explained variance, they were selected as the primary modelling approach in our study. In addition, random forests can handle high-dimensional data structures and capture complex, non-linear relationships (Chang et al., 2023; Jevšenak and Skudnik, 2021).

The models were calibrated at three different levels of complexity. The first level represents a model including all TRW data independent of forest type or species. The second level consists of three different models representing the three different forest-type classifications as obtained from the CORINE land cover classification (coniferous, broadleaved and mixed forest). The third level of complexity comprises eight species-specific models, representing the eight abundant tree species (*Abies alba*, *Picea abies*, *Pinus sylvestris*, *Pinus nigra*, *Pseudotsuga meziesii*, *Fagus sylvatica*, *Quercus petraea* and *Quercus robur*).

At each level, we first reduced the initial pool of 127 potential independent variables by removing collinear variables with a Pearson correlation coefficient above 0.70 (Dormann et al., 2013). If two independent variables had a correlation that was stronger than 0.70, we retained the one that had a higher correlation score with TRW. To assess the importance of each predictor variable in contributing to the model's predictive performance, we employed the *cforest()* function from the R package *party* version 1-3-11 (Strobl et al., 2008) to compute the conditional variable importance. To establish relative importance, we normalised these values by dividing the conditional variable importance by the sum of importance within each model, providing a comprehensive assessment of the predictors' overall impact. All variables with a relative importance of <1 % were removed. All remaining variables were used to fit the random forest models with the R package ranger version 0.13.1 (Wright and Ziegler, 2015).

To evaluate the relative contribution of the remote sensing variables in comparison to climate and elevation in explaining the dependent variable TRW (Objective 2), we evaluated and compared the model performance with and without the EOS data for each computed model (i.e. for all sites, forest type and species specific). To test whether differences in explained variance (ΔR^2) were significantly different from 0, we employed the Wilcoxon signed-rank test (Harris and Hardin, 2013). In the event that the EOS data did not improve the explained variance in the independent data, the final selected model was fitted without the EOS data. The marginal effect of the predictor variables on tree growth was derived from partial dependence plots for each model (Greenwell, 2017). To do so, the predictor variables were simulated for a range of existing values, while all the other numerical variables were kept constant based on their medians.

Model validation was done using *k*-fold spatially blocked cross-validation, where models are systematically trained using *k-1* folds and validated based on the remaining fold. Blocked cross-validation is a robust validation approach for models with spatial structures (Bergmeir and Benítez, 2012). To assess the impact of the proportion of training data used, we evaluated a range of *k* values from 5 to 50. For each model, we analysed the residual structure (Supplementary Fig. 3) and calculated the explained variance (R^2), root mean square error (RMSE; Pham et al., 2022) and root relative square error (RRSE; Pham et al., 2022).

2.5. Forest-type model upscaling

To demonstrate model upscaling at a coarse resolution and to identify critical gaps in model spatial applicability (Objective 3), the three forest-type models were applied to predict annual TRW in the region represented by TREOS. For this purpose, we created a 0.05-degree spatial resolution grid covering the region between latitudes 40°N and 60°N and longitudes 5°E and 30°E. For each grid point, we first

extracted the CORINE land cover (Büttner, 2014) information and retained only the forest-covered grid points for further analyses. For these, we then extracted all the required predictor variables derived from the forest-type models and predicted TRW for the year 2021. For each of the three forest types – coniferous, broadleaves and mixed – we made predictions and summarised them in a map. An important limitation of this approach is the extraction of EOS data, which was derived only for the grid centre with a radius of 100 m and is thus not representative of all the pixels. Therefore, this upscaling serves only as a general demonstration of the model's applicability across space. To identify where models cannot generate reliable predictions, we applied the principle of 'area of applicability' (AOA) using the CAST R package version 0.6.0 (Meyer and Pebesma, 2021), which identifies pixels for which model predictions are supported by available training data, preventing unreliable spatial extrapolations. Finally, we analysed the distribution of the key predictor variables within and outside the AOA to identify the critical prediction space, which is defined as the area where the predictor variables are underrepresented, providing guidance for future sampling campaigns.

3. Results and discussion

3.1. Earth observation by satellites (EOS) data increases the prediction accuracy of tree-ring width (TRW)

Incorporating EOS data significantly improved model performance. In particular, it increased the prediction accuracy (ΔR^2) of TRW by 0.06 on average (Supplementary Fig. 1, Table 1) and reached a maximum ΔR^2 of 0.11 for the coniferous and mixed forest models. ΔR^2 was negatively related to climate. For species for which growth was only poorly explained by climate variables, the incorporation of EOS data yielded stronger improvement regarding the growth model.

Among the predictor variables, EOS had a relative importance (Strobl et al., 2007) of up to 84 % (mixed forests), while for climate variables and elevation, it was the highest for *Quercus petraea* (94 %) and broadleaved forests (41 %), respectively. However, the relative importance of EOS varied considerably among the models (Fig. 2, Supplementary Table 1). For the general model, the total relative variable importance of EOS was 54 %. A high variable importance of EOS was also obtained for coniferous forests (63 %). However, for broadleaved forests, EOS incorporation did not improve the model performance. At the species level, EOS relative importance was high for *Pinus nigra* (60 %) and *Picea abies* (56 %) but did not add any additional information for *Quercus petraea* and *Pseudotsuga menziesii*. For the remaining species, EOS importance ranged from 14 % (*Quercus robur*) up to 52 % (*Pinus sylvestris*), with a tendency towards lower EOS importance for broadleaved tree species (Fig. 2).

Table 1
Comparison of the explained variance (R^2) in models for predicting tree-ring width (TRW) with and without Earth observation by satellites (EOS), along with the resulting differences denoted as ΔR^2. Statistical significance was assessed using the *p*-value from the Wilcoxon signed-rank test, indicating differences from zero. The explained variance was calculated using the independent data from *k*–fold blocked cross-validation, where *k* ranged from 5 to 50 with a step of 5.

Model	R^2 with EOS	R^2 without EOS	ΔR^2
General model	0.15	0.06	0.09 ($p < 0.002$)
Coniferous Forest	0.20	0.09	0.11 ($p < 0.002$)
Broadleaved Forest	0.15	0.17	−0.02 ($p < 0.002$)
Mixed Forest	0.12	0.02	0.11 ($p < 0.002$)
Abies alba	0.24	0.25	0.00 ($p < 0.375$)
Picea abies	0.25	0.16	0.09 ($p < 0.002$)
Pinus nigra	0.40	0.39	0.02 ($p < 0.846$)
Pinus sylvestris	0.21	0.16	0.05 ($p < 0.020$)
Pseudotsuga menziesii	0.07	0.21	−0.14 ($p < 0.002$)
Fagus sylvatica	0.22	0.15	0.07 ($p < 0.002$)
Quercus petraea	0.40	0.45	−0.05 ($p < 0.002$)
Quercus robur	0.36	0.33	0.03 ($p < 0.064$)

All the EOS variables yielded positive relationships with TRW (Supplementary Fig. 2). This alignment is consistent with previously documented observations indicating that the NDVI, EVI and NDRE tend to increase with higher photosynthetic activity (Xue and Su, 2017), making them reliable indicators of growth. Notably, among the EOS variables, the NDMI emerged as the most important predictor variable. This prominence can be attributed to its capacity to capture canopy roughness and water content, both of which exert a substantial influence on photosynthetic activity and, consequently, tree growth. The NDMI mirrors plant–water status, directly linked to carbon assimilation rates and, thus, secondary growth (Castagneri et al., 2022; Dobbertin, 2005). Furthermore, its utility extends beyond growth assessment, as studies have demonstrated its effectiveness in detecting deforestation (Schultz et al., 2016), mapping bark beetle outbreaks (Havašová et al., 2015) and delineating rubber plantations (Fan et al., 2015).

In six (seven) out of the twelve models, the EVI (NDRE) provided additional information but had lower importance in comparison to the NDMI and SAR. This outcome was unexpected, given that both EVI and NDRE are closely linked to vegetation vigour. The EVI was designed to correct for atmospheric conditions and canopy background noise and is, when compared to the NDVI, less prone to saturation (Huete et al., 2002) and more sensitive to changes in vegetation condition in areas with dense vegetation (Boegh et al., 2002). The NDRE, utilising red-edge bands in its formulation, is well-suited for estimating canopy chlorophyll and is strongly associated with vegetation stress (Clevers and Gitelson, 2013), a factor known to significantly reduce secondary growth. The NDVI, which is traditionally used to detect and evaluate forest growth trends, was not selected by any of the models. We suggest that the information inherent in the NDVI is likely represented by the combination of other indices (e.g. NDRE) and climate variables, all of which are known to exhibit significant correlations with the NDVI (Piao et al., 2014). The NDMI emerged as the most crucial proxy for predicting TRW in our network, underscoring its importance in future studies focused on mapping forest growth.

SAR variables were included in eight out of the twelve models, and the relative importance of these variables was 13 % on average, with the largest relative importance obtained for *Pinus nigra* (28 %). The RVI had a consistent positive relationship with tree growth in mixed forests (Supplementary Fig. 2, panel h), which agrees with other studies showing that the RVI increases with higher vegetation growth and has enhanced sensitivity to vegetation cover and biomass (Szigarski et al., 2018). Several studies have successfully established connections between Sentinel-1 backscatter dynamics and biophysical parameters of crops such as wheat and soybean (Mandal et al., 2020), as well as vegetation dynamics (Vreugdenhil et al., 2018) and height (Bartsch et al., 2020). This underscores the versatility of SAR variables, highlighting their significant role in elucidating the variability in TRWs. Overall, the inclusion of SAR variables in our models contributes valuable insights into the complex interplay between vegetation and tree growth dynamics.

The relative importance of climate variables varied significantly among the different models, as illustrated in Fig. 2 and detailed in Supplementary Table 1. Mean growing season temperature and precipitation sums had similar importance, while climatic water balance – combining precipitation with evapotranspiration – was less important. This implies that actual precipitation plays a more pivotal role than drought status across the entire considered gradient. Seasonal temperature was more significant for oak species and *Pinus nigra*, while precipitation was more significant for *Pseudotsuga menziesii* and *Abies alba*. Nevertheless, both factors consistently exerted a strong positive influence on tree growth (Supplementary Fig. 2), highlighting that warm and wet conditions generally favour tree growth. Elevation featured in eleven out of the twelve models; however, its impact on the dependent variable, TRW, exhibited a mixed pattern. The influence ranged from

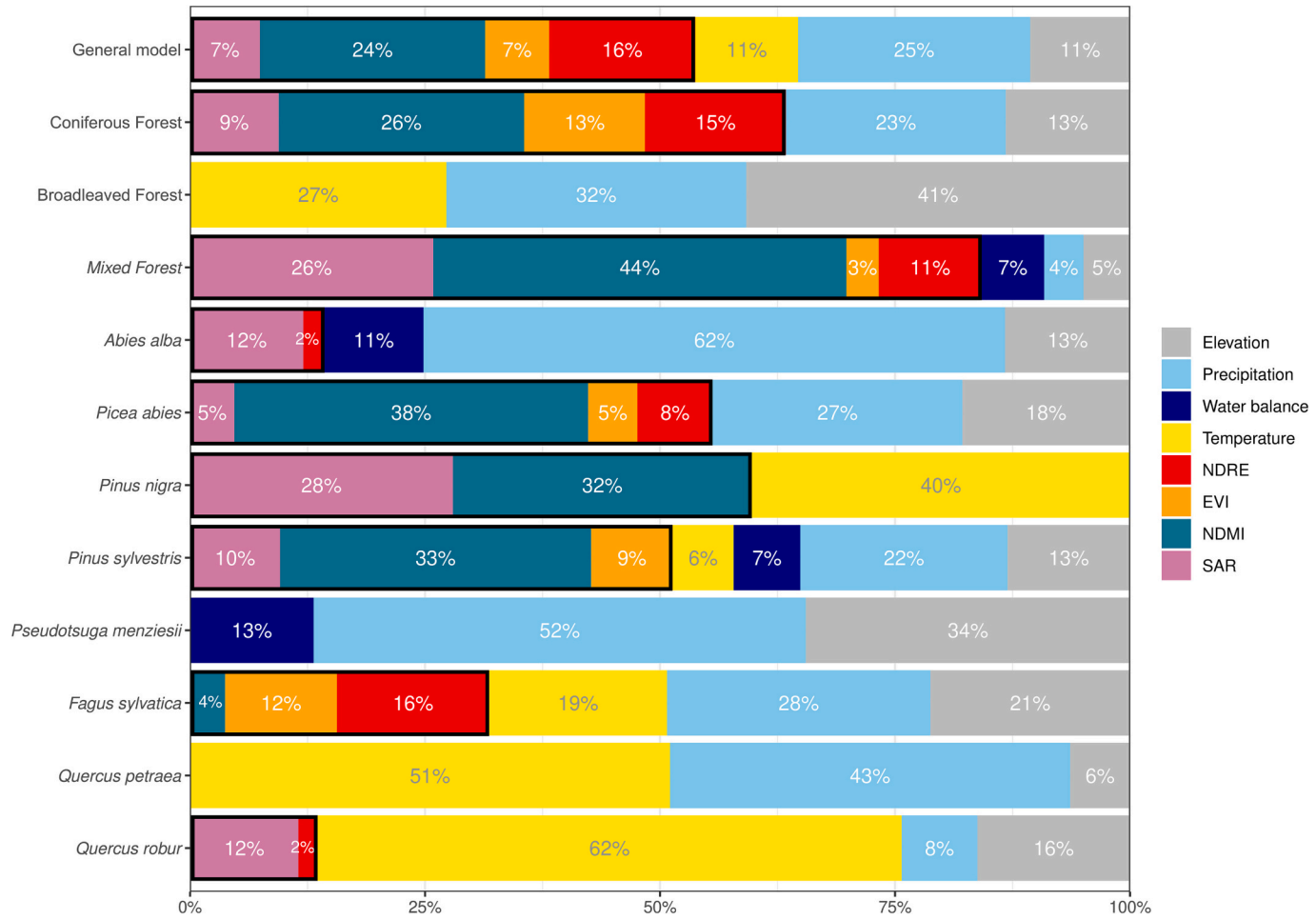

Fig. 2. The relative importance of predictor variables on tree-ring width (TRW). To enhance readability, we combined different seasonal aggregates and long-term averages of climate variables in one group. EOS-related variables are highlighted with a bold rectangle. More detailed statistics for each variable are in Supplementary Table 1. NDRE – normalised difference red edge index, EVI – enhanced vegetation index, NDMI – normalised difference moisture index, SAR – synthetic aperture radar variables.

positive for *Fagus sylvatica*, as depicted in Supplementary Fig. 2, panel s, to negative for *Quercus robur*, as illustrated in Supplementary Fig. 2, panel x. This intricate orographic interaction, coupled with the different optimal seasons related to climate variables, likely mirrors a broad spatial gradient and the diverse ecophysiological preferences of the included species (King et al., 2013; Ponocná et al., 2016).

3.2. The importance of species and site for predicting tree-ring width (TRW)

Among all the models constructed, 13–52 % of the annual variance in TRW was explained by the predictor variables tested (Fig. 3). The predictor variables explained the highest amount of variance in TRW in species-specific models. In models for broadleaved and coniferous forests, predictor variables explained roughly the same amount of variance in TRW (19 % vs. 21 %, respectively), while the model for mixed forests performed comparably worse (R^2 = 13 %). These findings align with expectations, as forests with more homogeneous compositions, such as coniferous and broadleaved forests, tend to possess simpler vertical structures and growth dynamics (Franklin, 1986). This simplicity necessitates fewer independent variables, making predictions more straightforward. Furthermore, the relatively low model performance for mixed forests is not surprising, given that each site was solely characterised by species-specific chronology. Consequently, the intricate composition of species mixtures within mixed forests was not adequately represented in our tree-ring network. Although it has already been shown that different species can be combined in site chronologies for analyses of tree growth, because they respond similarly to fluctuations in climate variables (Klisz et al., 2023; Opała and Mendecki, 2014), this approach still needs to be evaluated in terms of comparison with data from EOS.

Among the species-specific models, the best performance was observed for *Pinus nigra* (R^2 = 0.45) and *Quercus petraea* (R^2 = 0.52), which had the lowest numbers of input chronologies (Fig. 1a). Good model performance was also obtained for *Quercus robur* (R^2 = 0.40), with TRW data predominantly originating from mono-specific stands, potentially resulting in simplified tree growth patterns due to a lack of inter-species competition. In contrast, increased competition for sunlight, nutrients and water reduces growth rates of individual trees (Coomes and Allen, 2007; Jevšenak and Skudnik, 2021) and thus also the performance of models where competition is not included. The model for *Pseudotsuga menziesii* was based on sub-populations from high elevation sites from the Balkan Peninsula and Switzerland and a sub-Mediterranean provenance trial, as well as many sites close to the Baltic Sea and central Poland (Fig. 1). These highly diverse sampled sites with limited replication likely exhibit very different vegetation dynamics that was not properly accounted for in our modelling approach, resulting in lower model performance. However, even for the highly diverse data of *P. menziesii*, we obtained reasonably accurate predictions when the share of the training data was above 95 % (Supplementary Fig. 1), ensuring sufficient training data for the models to robustly learn the link between tree growth and the input variables.

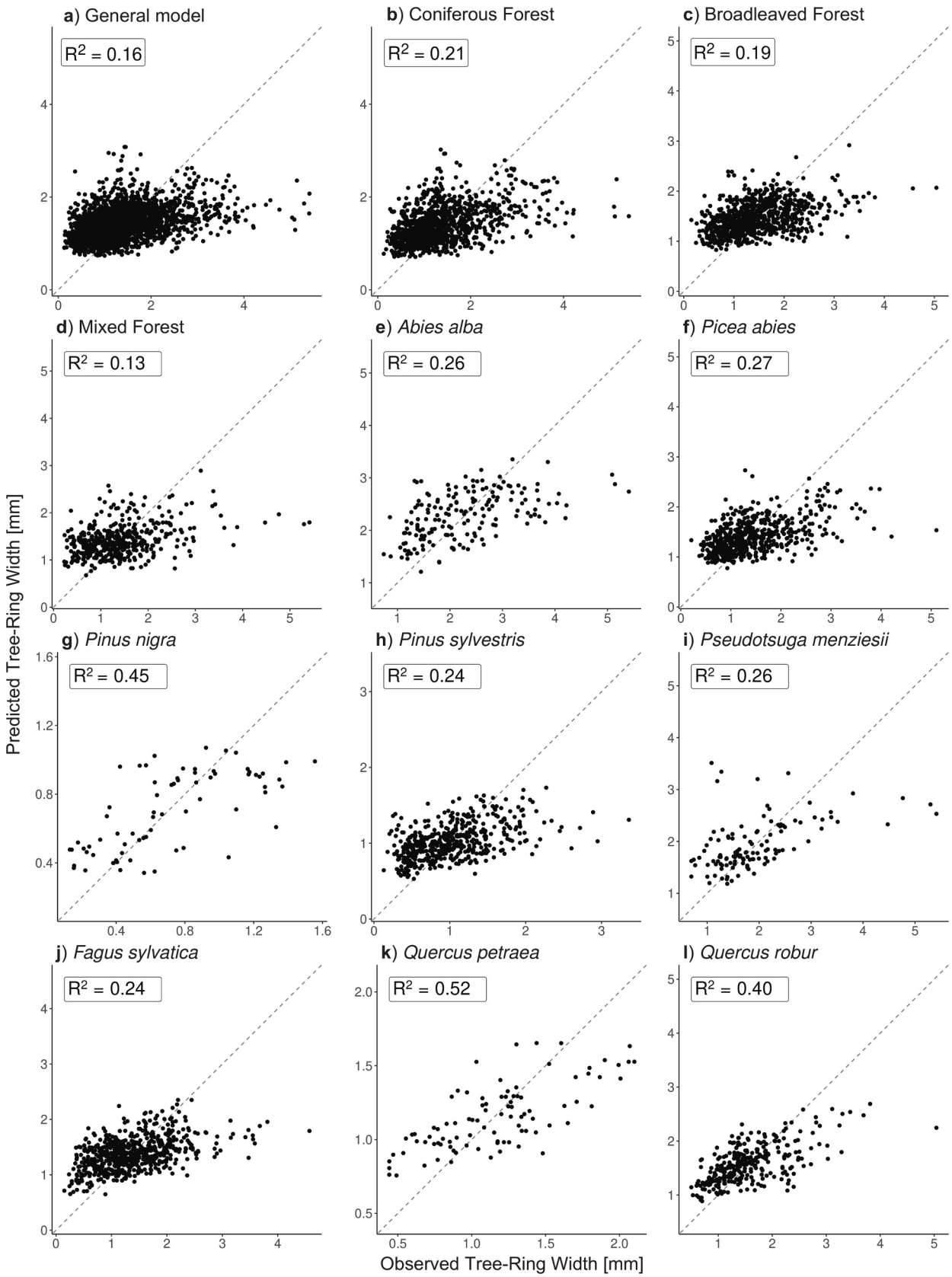

Fig. 3. Scatterplots of predicted and observed ring widths with the indicated mean explained variance (R^2) across all *k*-fold cross-validations. To highlight the robustness of the models, we strictly report the statistics derived from the model validation. The R^2, root mean square error (RMSE) and root relative square error (RRSE) for specific *k*-folds are reported in Supplementary Fig. 1. The dashed line indicates a perfect 1-1 regression.

In contrast to the less specific models, which include all sites and forest types, the species-specific models show a significantly higher explained variance. This clearly underlines a preference for species-specific models, as they have a higher explanatory power, as shown in Fig. 3. However, it is essential to note that when applying these models for spatial predictions, adequate sample replication becomes crucial. The model performance experiences a significant decline for sparsely represented species, as exemplified by *Pseudotsuga menziesii* (Fig. 3). The importance of representative input data was also evident from the residual plot analyses (Supplementary Fig. 3), where we observed a moderate prediction bias for large TRWs, which were generally underestimated by the models. This bias could be removed by including additional stands with high productivity (Rahimzadeh-Bajgiran et al., 2020).

3.3. Upscaling tree growth for the three forest-type models

We used the principle of AOA to estimate regions in which the developed forest type models can be reliably applied to predict TRW (Meyer and Pebesma, 2021). The combined forest-type model predictions were applicable to a large part of our study region (73 %) (Fig. 4). The highest share of pixels within the AOA was calculated for mixed forests (87 %), while for coniferous and broadleaved forests it was lower – 77 % and 61 %, respectively (Supplementary Fig. 4). The area within the AOA greatly overlapped with the sampled locations (Fig. 1), where major gaps are found in Italy, the south-eastern Balkans and the Alps.

The distribution of key predictor variables within and outside the AOA (Supplementary Fig. 5) indicated that the coniferous model was not applicable to forests that had a low NDMI and NDRE and relatively higher late spring rainfall at high elevation sites. The model for broadleaved species, on the other hand, exhibited a high share of pixels outside the AOA when the long-term growing season temperature was relatively low or relatively high, with comparably lower summer precipitation and higher elevation. Taken together, the regions outside the AOA represent high-elevation sites and the spatial margins of the TREOS network. To fill the gaps outside the AOA, additional data should be collected in currently underrepresented areas.

Annual prediction maps of TRW on large scales are thus a distinctive opportunity for investigating the effects of environmental changes on tree growth. The creation and comparison of annual TRW maps provide a means for indirect assessment of extreme events, such as droughts (Jiao et al., 2021), heatwaves and bark beetle infestations (Bárta et al., 2022), with high resolution. Other approaches to mapping forest growth include national forest inventories (NFIs) and wood production statistics (Verkerk et al., 2015) or are based exclusively on climate data (Bodesheim et al., 2022) and thus have limited applicability. In our approach, we integrated three forest-type models; however, their explanatory power is constrained due to the uneven representation of different species. In an ideal scenario, the representation of different tree species in our forest-type models would accurately mirror their natural prevalence in the environment. The prediction accuracies can likely be substantially improved by deploying EOS-based tree-species classifications (Welle et al., 2022), which would allow for high-resolution species-specific growth predictions.

In order to extend our methodology to a species-level resolution and generate comprehensive maps of annual TRW across Europe, it is imperative to undertake additional data collection on a systematic grid. This grid should be designed to adequately capture the representativeness of the different tree species and forest types at a continental scale. Such sampling campaigns could be integrated into NFIs, in which tree ring data are often collected to estimate forest age and radial tree growth (Tomppo et al., 2010). The existing frameworks of NFIs present an ideal opportunity for such an initiative. The use of established NFI systems allows for the inclusion of additional site-specific information already collected, paving the way for the development of more accurate predictive models, not only for mapping TRW but also for basal area and volume increments.

3.4. Limitations

In our study, we employed Sentinel-1 and Sentinel-2 EOS data to model annual TRW. The high spatial resolution of both satellite sources is the main advantage of our approach. For instance, the pixel size of Sentinel-2 bands used in our study is 100–400 m^2, a significant improvement compared to the alternative Landsat 8 with a pixel size of 900 m^2 (Loveland and Irons, 2016). However, since Sentinel-2 revisit frequency of 5 days has only been available since March 2017, we had to restrict our analyses to the period 2017–2022. Despite the relatively short time series, this constraint was offset by the extensive spatial representation encompassing 707 sites, yielding a substantial dataset of 2686 data points for the modelling phase.

We focused on TRW, which is commonly considered a proxy for NPP (Dye et al., 2016; Wang et al., 2023). However, if using basal area increments (BAI) instead, predictions would be more closely related to the actual wood volume produced and thus more representative of actual forest biomass increase. However, for a large part of the TREOS network, stem diameters – which are needed for accurate BAI calculations – were not available. Due to this constraint, we decided to model secondary tree growth, as obtained from TRWs. Furthermore, focusing on stand biomass and/or wood volume increments would provide a more precise estimate of the actual NPP but would require an additional measure of height (apical) growth and basal area across the stand, which was not realised in this study. Finally, we want to stress the well-documented sampling bias, which is caused by the selection of dominant and mature trees, while sampling should be random to robustly estimate growth at the stand level (Nehrbass-Ahles et al., 2014).

To improve the prediction accuracy of the established models, additional variables could be considered. Variables related to site quality, such as soil depth, nutrient availability and soil water holding capacity, were not considered in our study. However, these factors are known to have a significant impact on tree growth (Durand et al., 2020; Kostić et al., 2021) and can be approximated by tree height, which can be obtained from the Global Ecosystem Dynamics Investigation (GEDI) (Potapov et al., 2021). Tree competition is one of the most significant factors related to tree growth (Jiang et al., 2018; Zhang et al., 2015), but it was not included in our study due to missing stand and tree size variables. Severe droughts, such as observed in 2003 and 2018 in central Europe (Buras et al., 2020) have major effects on forest growth. These effects were partially considered in our study by employing climatic water balance, but strong legacy effects, which can last for several years (Anderegg et al., 2015) and possible indirect effects resulting in bark beetle attacks (Robbins et al., 2022), soil (Qing et al., 2023) and atmospheric drying (Churakova Sidorova et al., 2020) were not directly included in our modelling approach. However, for future campaigns focused on large-scale tree growth modelling, additional variables related to site characteristics, drought legacies and tree competition will likely increase the understanding of interactions between secondary tree growth, climate and EOS.

Finally, in regions with more frequent cloud cover, harmonised Sentinel-2 and Landsat 8 datasets (Claverie et al., 2018) could improve the calculation of seasonal vegetation indices and thus may increase the prediction accuracy of tree growth due to an improved representation of growing season conditions. In the future, longer EOS time series will be available, which may allow for incorporating possible carryover effects from the previous growing season as well as drought-induced growth legacies (Anderegg et al., 2015; Gričar et al., 2022; Lian et al., 2021).

4. Conclusions

In summary, we have shown that EOS is a valuable, high-resolution source of information that increases the accuracy of models for

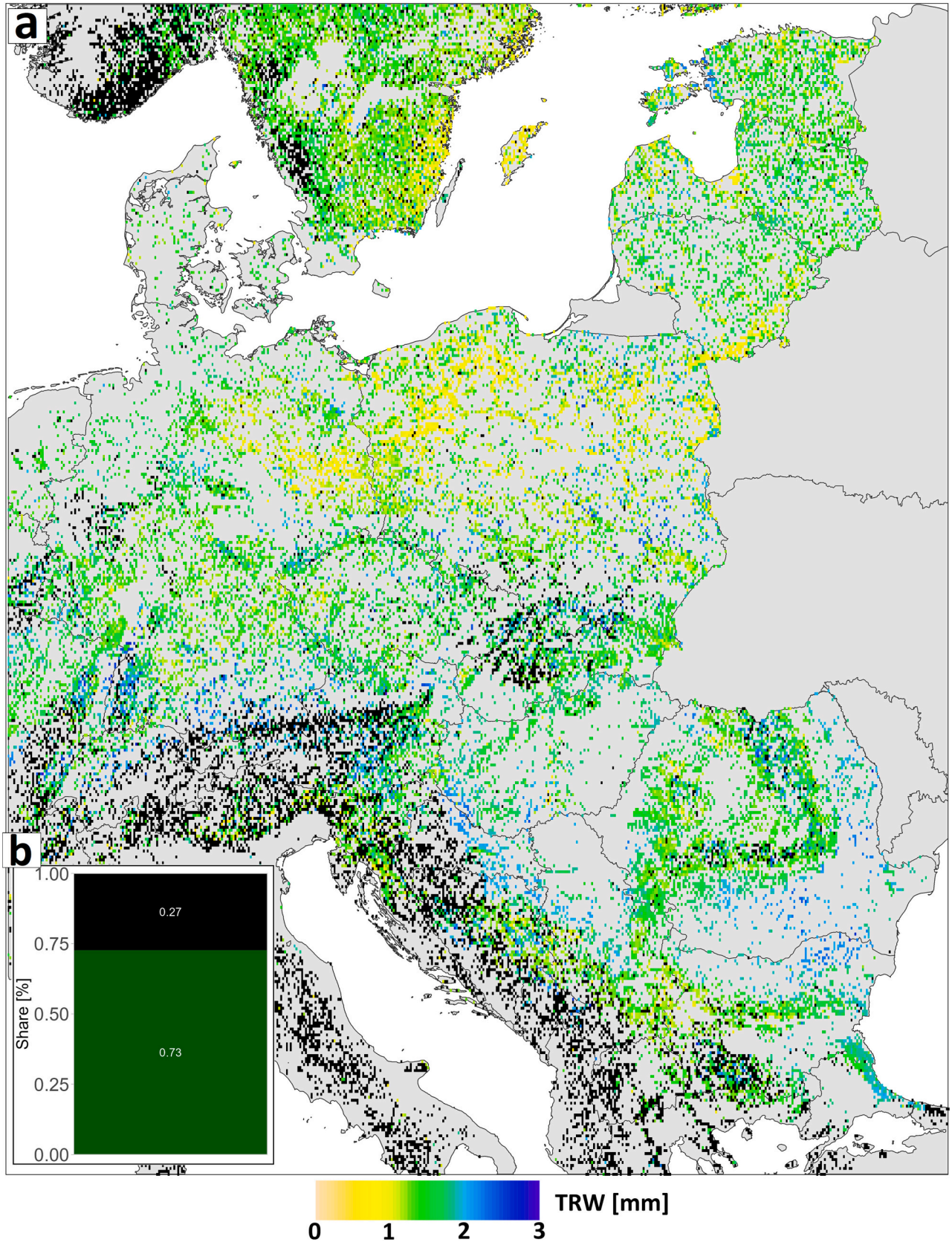

Fig. 4. Predicted tree-ring width (TRW) in 2021 for the three different CORINE land cover forest types at a spatial resolution of 0.05° (the mean cell size area ranges from roughly 12.5 to 24 km^2) (a), share of pixels within (green colour) and outside (black colour) the area of applicability (AOA) (b). Pixel colour refers to predicted tree-ring width ranging from yellow (low growth) to blue (high growth) colours. Black pixels indicate forests outside the area of applicability (AOA), where the predictions based on the current TREOS network are not reliable.

predicting tree-ring width. Most of the information added by EOS seems to relate to plant water status, as approximated by the NDMI. The inclusion of additional related vegetation indices further improved the prediction accuracy, since these indices are linked to canopy greenness and, thus, photosynthetic capacity (EVI) as well as plant stress (NDRE). In addition to the incorporation of optical EOS, our study highlights the added value of SAR data and, in particular, the RVI. However, the interpretation of the RVI is less straightforward because the signal can be associated with moisture, the leaf area index and other vegetation characteristics related to the forest density, competition and developmental stage. The maps produced in this study clearly indicate that our methodological approach can be used to produce high-resolution maps of annual secondary tree growth on a large scale and with unprecedented precision. Consequently, the incorporation of EOS into gridded forest growth products has the potential to improve our understanding of forests' climate-change resilience across large environmental gradients, thereby providing an important source of knowledge for forest managers, stakeholders and policy makers.

Funding

J.J. and A.B. were supported by the Alexander von Humboldt Postdoctoral Fellowship; J.J., K.O. and Mi.Sk. by the Slovenian Research Agency (ROVI – J2-3055); J.T. by Charles University (UNCE/HUM 018); Ma.Kl. by the Forest Research Institute, subsidy funds received from Polish Ministry of Education and Science, "Adaptive potential of silver fir and Douglas-fir in the gradient of the climatic conditions of northern Poland" (project no 90.02.47); J.E. and E.M.dC by the ERC Advanced Grant MONOSTAR (AdG 882727); K.J. by the BaltRap project (funded by the Leibniz Association) and the German Academic Exchange Service; T.Z. by project N№ KP-06-N№ 31/12 (financed by the Bulgarian National Science Fund); Ma.Kl., Ra.Pu., M.L. and Ma.Met. by the COST Action CA19128 (PEN-CAFoRR) "Pan-European Network for Climate Adaptive Forest Restoration and Reforestation" (funded by COST – European Cooperation in Science and Technology); Ra.Pu. by the Polish National Science Centre (2017/01/X/NZ8/00257); K.Č. and Ma.Mer. by the Slovenian Research Agency ARRS (programme P4-0015 "Wood and lignocellulosic composites"); N.Š.D. by the Slovenian Research Agency ARRS (young researchers' programme); J.J., Mi.Sk., Po.Ha. and T.L. by the Slovenian Research Agency ARRS (programme P4-0107 "Forest biology, ecology and technology"); J.G., L.K. and D.A. by the Slovenian Research Agency ARRS (programme P4-0430 "Forest-timber chain and climate change: the transition to a circular bioeconomy"); K.N. by AdFutura (257. JR) and the "Researchers-2.1-UL-BF-952011" project, contract no. C3330-19-952011, co-financed by the Ministry of Education, Science and Sport of the Republic of Slovenia and the EU European Regional Development Fund and by the Slovenian Research Agency (ARRS); Ma.Met. by the Estonian Research Council grant (PRG1586) and Estonian University of Life Sciences projects (P180024MIME and P200029MIME); D.Z. by the German Waldklimafonds (FKZ 28W-C-4-077-01); M.Á. and Z.K. by the National Research Development, and Innovation Office (NKFIH) through grant project no. FK 134547; C.R. by the Ministry of Research, Innovation and Digitisation, CNCS – UEFISCDI, project number PN-III-P1-1.1-TE-2021-1419, within PNCDI III; An.Po. and I.P. by the Ministry of Research, Innovation and Digitisation under project PN-III-P4-PCE-2021-1002 and CresPerfInst (34PFE/2021); Mi. Bo. by the Slovak Research and Development Agency via grant no. APVV-19-0183; T.K., Mi.Ry. and I.S. by the Czech Science Foundation (No. 23-07583S); Sa.Me. by the Estonian Environmental Investment Centre and Estonian University of Life Sciences (project P200189MIMP); Pe.Ho., J.K., and Ja.Sv. by the EEA Grants and the KAPPA programme (TO01000345); Pe.Ho., J.K., J.S. and Ma.St. by the CzecOS programme (LM2023048); B.S. and C.Z. by the German Research Foundation (SCHU 2935/2-1, ZA 755/2-1), and I.M. by the National Research Development, and Innovation Office (NKFIH) through grant project no. SNN 125652.

CRediT authorship contribution statement

Jernej Jevšenak: Conceptualization, Data curation, Formal analysis, Funding acquisition, Visualization, Writing – original draft, Writing – review & editing. **Marcin Klisz:** Data curation, Writing – review & editing. **Jiří Mašek:** Data curation. **Vojtěch Čada:** Data curation. **Pavel Janda:** Data curation. **Miroslav Svoboda:** Data curation. **Ondřej Vostarek:** Data curation. **Vaclav Treml:** Data curation. **Ernst van der Maaten:** Data curation, Writing – review & editing. **Andrei Popa:** Data curation. **Ionel Popa:** Data curation. **Marieke van der Maaten-Theunissen:** Data curation, Writing – review & editing. **Tzvetan Zlatanov:** Data curation. **Tobias Scharnweber:** Data curation. **Svenja Ahlgrimm:** Data curation. **Juliane Stolz:** Data curation, Writing – review & editing. **Irena Sochová:** Data curation. **Cătălin-Constantin Roibu:** Data curation. **Hans Pretzsch:** Data curation, Writing – review & editing. **Gerhard Schmied:** Data curation. **Enno Uhl:** Data curation. **Ryszard Kaczka:** Data curation. **Piotr Wrzesiński:** Data curation. **Martin Šenfeldr:** Data curation. **Marcin Jakubowski:** Data curation. **Jan Tumajer:** Data curation, Writing – review & editing. **Martin Wilmking:** Data curation. **Nikolaus Obojes:** Data curation. **Michal Rybníček:** Data curation. **Mathieu Lévesque:** Data curation, Writing – review & editing. **Aleksei Potapov:** Data curation, Writing – review & editing. **Soham Basu:** Data curation. **Marko Stojanović:** Data curation. **Stefan Stjepanović:** Data curation. **Adomas Vitas:** Data curation. **Domen Arnič:** Data curation. **Sandra Metslaid:** Data curation, Writing – review & editing. **Anna Neycken:** Data curation. **Peter Prislan:** Data curation. **Claudia Hartl:** Data curation. **Daniel Ziche:** Data curation, Writing – review & editing. **Petr Horáček:** Data curation. **Jan Krejza:** Data curation. **Sergei Mikhailov:** Data curation. **Jan Světlík:** Data curation. **Aleksandra Kalisty:** Data curation. **Tomáš Kolář:** Data curation. **Vasyl Lavnyy:** Data curation. **Maris Hordo:** Data curation. **Walter Oberhuber:** Data curation. **Tom Levanič:** Data curation. **Ilona Mészáros:** Data curation. **Lea Schneider:** Data curation. **Jiří Lehejček:** Data curation. **Rohan Shetti:** Data curation. **Michal Bošeľa:** Data curation, Writing – review & editing. **Paul Copini:** Data curation. **Marcin Koprowski:** Data curation. **Ute Sass-Klaassen:** Data curation, Writing – review & editing. **Şule Ceyda Izmir:** Data curation. **Remigijus Bakys:** Data curation. **Hannes Entner:** Data curation. **Jan Esper:** Data curation. **Karolina Janecka:** Data curation. **Edurne Martinez del Castillo:** Data curation. **Rita Verbylaite:** Data curation. **Mátyás Árvai:** Data curation. **Justine Charlet de Sauvage:** Data curation. **Katarina Čufar:** Data curation. **Markus Finner:** Data curation. **Torben Hilmers:** Data curation. **Zoltán Kern:** Data curation, Writing – review & editing. **Klemen Novak:** Data curation. **Radenko Ponjarac:** Data curation. **Radosław Puchałka:** Data curation. **Bernhard Schuldt:** Data curation. **Nina Škrk Dolar:** Data curation. **Vladimir Tanovski:** Data curation. **Christian Zang:** Data curation. **Anja Žmegač:** Data curation. **Cornell Kuithan:** Data curation. **Marek Metslaid:** Data curation. **Eric Thurm:** Data curation. **Polona Hafner:** Data curation. **Luka Krajnc:** Data curation. **Mauro Bernabei:** Data curation. **Stefan Bojić:** Data curation. **Robert Brus:** Data curation. **Andreas Burger:** Data curation. **Ettore D'Andrea:** Data curation. **Todor Đorem:** Data curation. **Mariusz Gławęda:** Data curation. **Jožica Gričar:** Data curation. **Marko Gutalj:** Data curation. **Emil Horváth:** Data curation. **Saša Kostić:** Data curation. **Bratislav Matović:** Data curation. **Maks Merela:** Data curation. **Boban Miletić:** Data curation. **András Morgós:** Data curation. **Rafał Paluch:** Data curation. **Kamil Pilch:** Data curation. **Negar Rezaie:** Data curation. **Julia Rieder:** Data curation. **Niels Schwab:** Data curation. **Piotr Sewerniak:** Data curation. **Dejan Stojanović:** Data curation. **Tobias Ullmann:** Data curation, Writing – review & editing. **Nella Waszak:** Data curation. **Ewa Zin:** Data curation. **Mitja Skudnik:** Data curation. **Krištof Oštir:** Data curation, Writing – review & editing. **Anja Rammig:** Data curation, Writing – review & editing. **Allan Buras:** Conceptualization, Data curation, Funding acquisition, Methodology, Supervision, Validation, Writing – review & editing.

Declaration of competing interest

The authors declare no competing interests.

Data availability

Data will be made available on request.

Acknowledgements

Nikolaus Obojes acknowledges the help of Jennifer Klemm in the sample collection and preparation.

Appendix A. Supplementary data

Supplementary data to this article can be found online at https://doi.org/10.1016/j.scitotenv.2023.169692.

References

Anderegg, W.R., Schwalm, C., Biondi, F., Camarero, J.J., Koch, G., Litvak, M., et al., 2015. Pervasive drought legacies in forest ecosystems and their implications for carbon cycle models. Science 349, 528–532.
Andreu-Hayles, L., D'Arrigo, R., Anchukaitis, K.J., Beck, P.S., Frank, D., Goetz, S., 2011. Varying boreal forest response to Arctic environmental change at the Firth River, Alaska. Environ. Res. Lett. 6, 045503.
Babst, F., Bodesheim, P., Charney, N., Friend, A.D., Girardin, M.P., Klesse, S., et al., 2018. When tree rings go global: challenges and opportunities for retro- and prospective insight. Quat. Sci. Rev. 197, 1–20.
Bárta, V., Hanuš, J., Dobrovolný, L., Homolová, L., 2022. Comparison of field survey and remote sensing techniques for detection of bark beetle-infested trees. For. Ecol. Manag. 506, 119984.
Bartsch, A., Widhalm, B., Leibman, M., Ermokhina, K., Kumpula, T., Skarin, A., et al., 2020. Feasibility of tundra vegetation height retrieval from Sentinel-1 and Sentinel-2 data. Remote Sens. Environ. 237, 111515.
Beck, P.S.A., Andreu-Hayles, L., D'Arrigo, R., Anchukaitis, K.J., Tucker, C.J., Pinzón, J.E., et al., 2013. A large-scale coherent signal of canopy status in maximum latewood density of tree rings at arctic treeline in North America. Glob. Planet. Chang. 100, 109–118.
Bergmeir, C., Benítez, J.M., 2012. On the use of cross-validation for time series predictor evaluation. Inf. Sci. 191, 192–213.
Bhuyan, U., Zang, C., Vicente-Serrano, S.M., Menzel, A., 2017. Exploring relationships among tree-ring growth, climate variability, and seasonal leaf activity on varying timescales and spatial resolutions. Remote Sens. 9, 526.
Bodesheim, P., Babst, F., Frank, D., Hartl, C., Zang, C., Jung, M., et al., 2022. Predicting spatiotemporal variability in radial tree growth at the continental scale with machine learning. Environ. Data Sci. 1.
Boegh, E., Soegaard, H., Broge, N., Hasager, C.B., Jensen, N.O., Schelde, K., et al., 2002. Airborne multispectral data for quantifying leaf area index, nitrogen concentration, and photosynthetic efficiency in agriculture. Remote Sens. Environ. 81, 179–193.
Bonney, M.T., He, Y., 2021. Temporal connections between long-term Landsat time-series and tree-rings in an urban–rural temperate forest. Int. J. Appl. Earth Obs. Geoinf. 103, 102523.
Brehaut, L., Danby, R.K., 2018. Inconsistent relationships between annual tree ring-widths and satellite-measured NDVI in a mountainous subarctic environment. Ecol. Indic. 91, 698–711.
Bugmann, H., Brang, P., Elkin, C., Henne, P., Jakoby, O., Lévesque, M., et al., 2014. Climate Change Impacts on Tree Species, Forest Properties, and Ecosystem Services, pp. 79–90.
Buras, A., Rammig, A., Zang, C.S., 2020. Quantifying impacts of the 2018 drought on European ecosystems in comparison to 2003. Biogeosciences 17, 1655–1672.
Büttner, G., 2014. CORINE land cover and land cover change products. In: Manakos, I., Braun, M. (Eds.), Land Use and Land Cover Mapping in Europe, 18. Springer, Dordrecht, pp. 55–74.
Castagneri, D., Vacchiano, G., Hacket-Pain, A., DeRose, R.J., Klein, T., Bottero, A., 2022. Meta-analysis reveals different competition effects on tree growth resistance and resilience to drought. Ecosystems 25, 30–43.
Chang, X., Xing, Y., Gong, W., Yang, C., Guo, Z., Wang, D., et al., 2023. Evaluating gross primary productivity over 9 ChinaFlux sites based on random forest regression models, remote sensing, and eddy covariance data. Sci. Total Environ. 875, 162601.
Churakova Sidorova, O.V., Corona, C., Fonti, M.V., Guillet, S., Saurer, M., Siegwolf, R.T. W., et al., 2020. Recent atmospheric drying in Siberia is not unprecedented over the last 1,500 years. Sci. Rep. 10, 15024.
Claverie, M., Ju, J., Masek, J.G., Dungan, J.L., Vermote, E.F., Roger, J.-C., et al., 2018. The harmonized Landsat and Sentinel-2 surface reflectance data set. Remote Sens. Environ. 219, 145–161.
Clevers, J.G.P.W., Gitelson, A.A., 2013. Remote estimation of crop and grass chlorophyll and nitrogen content using red-edge bands on Sentinel-2 and -3. Int. J. Appl. Earth Obs. Geoinf. 23, 344–351.
Collalti, A., Ibrom, A., Stockmarr, A., Cescatti, A., Alkama, R., Fernández-Martínez, M., et al., 2020. Forest production efficiency increases with growth temperature. Nat. Commun. 11, 5322.
Coomes, D.A., Allen, R.B., 2007. Effects of size, competition and altitude on tree growth. J. Ecol. 95, 1084–1097.
Coops, N., Waring, R., 2001. Assessing forest growth across southwestern Oregon under a range of current and future global change scenarios using a process model, 3-PG. Glob. Chang. Biol. 7, 15–29.
Coops, N.C., Tompalski, P., Goodbody, T.R.H., Queinnec, M., Luther, J.E., Bolton, D.K., et al., 2021. Modelling lidar-derived estimates of forest attributes over space and time: a review of approaches and future trends. Remote Sens. Environ. 260, 112477.
Cornes, R.C., van der Schrier, G., van den Besselaar, E.J.M., Jones, P.D., 2018. An ensemble version of the E-OBS temperature and precipitation data sets. J. Geophys. Res. Atmos. 123, 9391–9409.
Correa-Díaz, A., Silva, L., Horwath, W., Gómez-Guerrero, A., Vargas-Hernández, J., Villanueva-Díaz, J., et al., 2019. Linking remote sensing and dendrochronology to quantify climate-induced shifts in high-elevation forests over space and time. J. Geophys. Res. Biogeosci. 124, 166–183.
Decuyper, M., Chávez, R.O., Čufar, K., Estay, S.A., Clevers, J.G.P.W., Prislan, P., et al., 2020. Spatio-temporal assessment of beech growth in relation to climate extremes in Slovenia – an integrated approach using remote sensing and tree-ring data. Agric. For. Meteorol. 287, 107925.
Dobbertin, M., 2005. Tree growth as indicator of tree vitality and of tree reaction to environmental stress: a review. Eur. J. For. Res. 124, 319–333.
Dorado-Liñán, I., Ayarzagüena, B., Babst, F., Xu, G., Gil, L., Battipaglia, G., et al., 2022. Jet stream position explains regional anomalies in European beech forest productivity and tree growth. Nat. Commun. 13, 2015.
Dormann, C.F., Elith, J., Bacher, S., Buchmann, C., Carl, G., Carré, G., et al., 2013. Collinearity: a review of methods to deal with it and a simulation study evaluating their performance. Ecography 36, 27–46.
Durand, M., Rose, C., Dupouey, J.-L., Legout, A., Ponton, S., 2020. Do tree rings record changes in soil fertility? Results from a Quercus petraea fertilization trial. Sci. Total Environ. 712, 136148.
Dye, A., Barker Plotkin, A., Bishop, D., Pederson, N., Poulter, B., Hessl, A., 2016. Comparing tree-ring and permanent plot estimates of aboveground net primary production in three eastern U.S. forests. Ecosphere 7, e01454.
Fan, H., Fu, X., Zhang, Z., Wu, Q., 2015. Phenology-based vegetation index differencing for mapping of rubber plantations using Landsat OLI data. Remote Sens. 7, 6041–6058.
Franklin, J., 1986. Thematic mapper analysis of coniferous forest structure and composition. Int. J. Remote Sens. 7, 1287–1301.
Fu, G., Sun, W., 2022. Temperature sensitivities of vegetation indices and aboveground biomass are primarily linked with warming magnitude in high-cold grasslands. Sci. Total Environ. 843, 157002.
Gallaun, H., Zanchi, G., Nabuurs, G.-J., Hengeveld, G., Schardt, M., Verkerk, P.J., 2010. EU-wide maps of growing stock and above-ground biomass in forests based on remote sensing and field measurements. For. Ecol. Manag. 260, 252–261.
Gang, C., Zhang, Y., Wang, Z., Chen, Y., Yang, Y., Li, J., et al., 2017. Modeling the dynamics of distribution, extent, and NPP of global terrestrial ecosystems in response to future climate change. Glob. Planet. Chang. 148, 153–165.
Gorelick, N., Hancher, M., Dixon, M., Ilyushchenko, S., Thau, D., Moore, R., 2017. Google Earth Engine: planetary-scale geospatial analysis for everyone. Remote Sens. Environ. 202, 18–27.
Gough, C.M., Atkins, J.W., Fahey, R.T., Hardiman, B.S., 2019. High rates of primary production in structurally complex forests. Ecology 100, e02864.
Greenwell, B.M., 2017. pdp: an R package for constructing partial dependence plots. R J. 9, 421.
Gričar, J., Jevšenak, J., Hafner, P., Prislan, P., Ferlan, M., Lavrič, M., et al., 2022. Climatic regulation of leaf and cambial phenology in Quercus pubescens: their interlinkage and impact on xylem and phloem conduits. Sci. Total Environ. 802, 149968.
Hargreaves, G.H., Samani, Z.A., 1982. Estimating potential evapotranspiration. J. Irrig. Drain. Div. 108, 225–230.
Harris, T., Hardin, J.W., 2013. Exact Wilcoxon signed-rank and Wilcoxon Mann–Whitney ranksum tests. Stata J. 13, 337–343.
Havašová, M., Bucha, T., Ferenčík, J., Jakuš, R., 2015. Applicability of a vegetation indices-based method to map bark beetle outbreaks in the High Tatra Mountains. Ann. For. Res. 295–310.
Ho, T.K., 1995. Random decision forests. In: Proceedings of 3rd International Conference on Document Analysis and Recognition, 1. IEEE, pp. 278–282.
Huete, A., Didan, K., Miura, T., Rodriguez, E.P., Gao, X., Ferreira, L.G., 2002. Overview of the radiometric and biophysical performance of the MODIS vegetation indices. Remote Sens. Environ. 83, 195–213.
Jevšenak, J., 2019. Daily climate data reveal stronger climate-growth relationships for an extended European tree-ring network. Quat. Sci. Rev. 221, 105868.
Jevšenak, J., Skudnik, M., 2021. A random forest model for basal area increment predictions from national forest inventory data. For. Ecol. Manag. 479, 118601.
Jiang, X., Huang, J.-G., Cheng, J., Dawson, A., Stadt, K.J., Comeau, P.G., et al., 2018. Interspecific variation in growth responses to tree size, competition and climate of western Canadian boreal mixed forests. Sci. Total Environ. 631, 1070–1078.
Jiao, W., Wang, L., McCabe, M.F., 2021. Multi-sensor remote sensing for drought characterization: current status, opportunities and a roadmap for the future. Remote Sens. Environ. 256, 112313.
Kaufmann, R., D'arrigo, R., Laskowski, C., Myneni, R., Zhou, L., Davi, N., 2004. The effect of growing season and summer greenness on northern forests. Geophys. Res. Lett. 31.

Keenan, R.J., 2015. Climate change impacts and adaptation in forest management: a review. Ann. For. Sci. 72, 145–167.
King, G.M., Gugerli, F., Fonti, P., Frank, D.C., 2013. Tree growth response along an elevational gradient: climate or genetics? Oecologia 173, 1587–1600.
Klisz, M., Puchałka, R., Jakubowski, M., Koprowski, M., Netsvetov, M., Prokopuk, Y., et al., 2023. Local site conditions reduce interspecific differences in climate sensitivity between native and non-native pines. Agric. For. Meteorol. 341, 109694.
Knapp, A.K., Smith, M.D., 2001. Variation among biomes in temporal dynamics of aboveground primary production. Science 291, 481–484.
Kostić, S., Wagner, W., Orlović, S., Levanič, T., Zlatanov, T., Goršić, E., et al., 2021. Different tree-ring width sensitivities to satellite-based soil moisture from dry, moderate and wet pedunculate oak (Quercus robur L.) stands across a southeastern distribution margin. Sci. Total Environ. 800, 149536.
Lian, X., Piao, S., Chen, A., Wang, K., Li, X., Buermann, W., et al., 2021. Seasonal biological carryover dominates northern vegetation growth. Nat. Commun. 12, 983.
Loveland, T.R., Irons, J.R., 2016. Landsat 8: the plans, the reality, and the legacy. Remote Sens. Environ. 185, 1–6.
Mandal, D., Kumar, V., Ratha, D., Dey, S., Bhattacharya, A., Lopez-Sanchez, J.M., et al., 2020. Dual polarimetric radar vegetation index for crop growth monitoring using sentinel-1 SAR data. Remote Sens. Environ. 247, 111954.
Martínez-Fernández, J., Almendra-Martín, L., De Luis, M., González-Zamora, A., Herrero-Jiménez, C., 2019. Tracking tree growth through satellite soil moisture monitoring: a case study of *Pinus halepensis* in Spain. Remote Sens. Environ. 235, 111422.
Mašek, J., Tumajer, J., Lange, J., Kaczka, R., Fišer, P., Treml, V., 2023. Variability in tree-ring width and NDVI responses to climate at a landscape level. Ecosystems 1–14.
Mašek, J., Tumajer, J., Lange, J., Vejpustková, M., Kašpar, J., Šamonil, P., et al., 2024. Shifting climatic responses of tree rings and NDVI along environmental gradients. Sci. Total Environ. 908, 168275.
Meyer, H., Pebesma, E., 2021. Predicting into unknown space? Estimating the area of applicability of spatial prediction models. Methods Ecol. Evol. 12, 1620–1633.
Morreale, L.L., Thompson, J.R., Tang, X., Reinmann, A.B., Hutyra, L.R., 2021. Elevated growth and biomass along temperate forest edges. Nat. Commun. 12, 7181.
Mullissa, A., Vollrath, A., Odongo-Braun, C., Slagter, B., Balling, J., Gou, Y., et al., 2021. Sentinel-1 SAR backscatter analysis ready data preparation in Google Earth Engine. Remote Sens. 13, 1954.
Nehrbass-Ahles, C., Babst, F., Klesse, S., Nötzli, M., Bouriaud, O., Neukom, R., et al., 2014. The influence of sampling design on tree-ring-based quantification of forest growth. Glob. Chang. Biol. 20, 2867–2885.
Opała, M., Mendecki, M.J., 2014. An attempt to dendroclimatic reconstruction of winter temperature based on multispecies tree-ring widths and extreme years chronologies (example of Upper Silesia, southern Poland). Theor. Appl. Climatol. 115, 73–89.
Pham, Q.B., Kumar, M., Di Nunno, F., Elbeltagi, A., Granata, F., Islam, A.R.M.T., et al., 2022. Groundwater level prediction using machine learning algorithms in a drought-prone area. Neural Comput. & Applic. 34, 10751–10773.
Piao, S., Nan, H., Huntingford, C., Ciais, P., Friedlingstein, P., Sitch, S., et al., 2014. Evidence for a weakening relationship between interannual temperature variability and northern vegetation activity. Nat. Commun. 5, 5018.
Pompa-García, M., Camarero, J.J., Colangelo, M., González-Cásares, M., 2021. Inter and intra-annual links between climate, tree growth and NDVI: improving the resolution of drought proxies in conifer forests. Int. J. Biometeorol. 65, 2111–2121.
Ponocná, T., Spyt, B., Kaczka, R., Büntgen, U., Treml, V., 2016. Growth trends and climate responses of Norway spruce along elevational gradients in East-Central Europe. Trees 30, 1633–1646.
Potapov, P., Li, X., Hernandez-Serna, A., Tyukavina, A., Hansen, M.C., Kommareddy, A., et al., 2021. Mapping global forest canopy height through integration of GEDI and Landsat data. Remote Sens. Environ. 253, 112165.
Qing, Y., Wang, S., Yang, Z.-L., Gentine, P., 2023. Soil moisture–atmosphere feedbacks have triggered the shifts from drought to pluvial conditions since 1980. Commun. Earth Environ. 4, 254.
Quillet, A., Peng, C., Garneau, M., 2010. Toward dynamic global vegetation models for simulating vegetation–climate interactions and feedbacks: recent developments, limitations, and future challenges. Environ. Rev. 18, 333–353.
Rahimzadeh-Bajgiran, P., Hennigar, C., Weiskittel, A., Lamb, S., 2020. Forest potential productivity mapping by linking remote-sensing-derived metrics to site variables. Remote Sens. 12, 2056.
Rehschuh, R., Mette, T., Menzel, A., Buras, A., 2017. Soil properties affect the drought susceptibility of Norway spruce. Dendrochronologia 45, 81–89.
Robbins, Z.J., Xu, C., Aukema, B.H., Buotte, P.C., Chitra-Tarak, R., Fettig, C.J., et al., 2022. Warming increased bark beetle-induced tree mortality by 30% during an extreme drought in California. Glob. Chang. Biol. 28, 509–523.
Salomón, R.L., Peters, R.L., Zweifel, R., Sass-Klaassen, U.G., Stegehuis, A.I., Smiljanic, M., et al., 2022. The 2018 European heatwave led to stem dehydration but not to consistent growth reductions in forests. Nat. Commun. 13, 28.
Schmitt, A., Trouvé, R., Seynave, I., Lebourgeois, F., 2020. Decreasing stand density favors resistance, resilience, and recovery of *Quercus petraea* trees to a severe drought, particularly on dry sites. Ann. For. Sci. 77, 1–21.
Schultz, M., Clevers, J.G.P.W., Carter, S., Verbesselt, J., Avitabile, V., Quang, H.V., et al., 2016. Performance of vegetation indices from Landsat time series in deforestation monitoring. Int. J. Appl. Earth Obs. Geoinf. 52, 318–327.
Speer, J.H., 2010. Fundamentals of Tree-ring Research. University of Arizona Press.
Stolz, J., van der Maaten, E., Kalanke, H., Martin, J., Wilmking, M., van der Maaten-Theunissen, M., 2021. Increasing climate sensitivity of beech and pine is not mediated by adaptation and soil characteristics along a precipitation gradient in northeastern Germany. Dendrochronologia 67, 125834.
Strobl, C., Boulesteix, A.-L., Zeileis, A., Hothorn, T., 2007. Bias in random forest variable importance measures: illustrations, sources and a solution. BMC Bioinforma. 8, 25.
Strobl, C., Boulesteix, A.-L., Kneib, T., Augustin, T., Zeileis, A., 2008. Conditional variable importance for random forests. BMC Bioinforma. 9, 1–11.
Szigarski, C., Jagdhuber, T., Baur, M., Thiel, C., Parrens, M., Wigneron, J.-P., et al., 2018. Analysis of the radar vegetation index and potential improvements. Remote Sens. 10, 1776.
Tian, Z., Yi, C., Fu, Y., Kutter, E., Krakauer, N.Y., Fang, W., et al., 2023. Fusion of multiple models for improving gross primary production estimation with eddy covariance data based on machine learning. J. Geophys. Res. Biogeosci. 128, e2022JG007122.
Tomppo, E., Gschwantner, T., Lawrence, M., McRoberts, R.E., Gabler, K., Schadauer, K., et al., 2010. National forest inventories. In: Pathways for Common Reporting. European Science Foundation, pp. 541–553.
Tsyganskaya, V., Martinis, S., Marzahn, P., Ludwig, R., 2018. Detection of temporary flooded vegetation using Sentinel-1 time series data. Remote Sens. 10, 1286.
Veci, L., Prats-Iraola, P., Scheiber, R., Collard, F., Fomferra, N., Engdahl, M., 2014. The sentinel-1 toolbox. In: Proceedings of the IEEE International Geoscience and Remote Sensing Symposium (IGARSS). IEEE, pp. 1–3.
Verkerk, P.J., Levers, C., Kuemmerle, T., Lindner, M., Valbuena, R., Verburg, P.H., et al., 2015. Mapping wood production in European forests. For. Ecol. Manag. 357, 228–238.
Vicente-Serrano, S.M., Camarero, J.J., Olano, J.M., Martín-Hernández, N., Peña-Gallardo, M., Tomás-Burguera, M., et al., 2016. Diverse relationships between forest growth and the Normalized Difference Vegetation Index at a global scale. Remote Sens. Environ. 187, 14–29.
Vicente-Serrano, S.M., Martín-Hernández, N., Camarero, J.J., Gazol, A., Sánchez-Salguero, R., Peña-Gallardo, M., et al., 2020. Linking tree-ring growth and satellite-derived gross primary growth in multiple forest biomes. Temporal-scale matters. Ecol. Indic. 108, 105753.
Vreugdenhil, M., Wagner, W., Bauer-Marschallinger, B., Pfeil, I., Teubner, I., Rüdiger, C., et al., 2018. Sensitivity of Sentinel-1 backscatter to vegetation dynamics: an Austrian case study. Remote Sens. 10, 1396.
Wang, T., Bao, A., Xu, W., Zheng, G., Nzabarinda, V., Yu, T., et al., 2023. Dynamics of forest net primary productivity based on tree ring reconstruction in the Tianshan Mountains. Ecol. Indic. 146, 109713.
Welle, T., Aschenbrenner, L., Kuonath, K., Kirmaier, S., Franke, J., 2022. Mapping dominant tree species of German forests. Remote Sens. 14, 3330.
Wigley, T.M.L., Jones, P.D., Briffa, K.R., 1987. Cross-dating methods in dendrochronology. J. Archaeol. Sci. 14, 51–64.
Wright, M.N., Ziegler, A., 2015. ranger: A Fast Implementation of Random Forests for High Dimensional Data in C++ and R. preprint at. https://arxiv.org/pdf/1508.04409.pdf.
Wu, C., Coffield, S.R., Goulden, M.L., Randerson, J.T., Trugman, A.T., Anderegg, W.R., 2023. Uncertainty in US forest carbon storage potential due to climate risks. Nat. Geosci. 1–8.
Wulder, M.A., Hermosilla, T., White, J.C., Coops, N.C., 2020. Biomass status and dynamics over Canada's forests: disentangling disturbed area from associated aboveground biomass consequences. Environ. Res. Lett. 15, 094093.
Xue, J., Su, B., 2017. Significant remote sensing vegetation indices: a review of developments and applications. J. Sens. 2017, 1353691.
Zhang, J., Huang, S., He, F., 2015. Half-century evidence from western Canada shows forest dynamics are primarily driven by competition followed by climate. Proc. Natl. Acad. Sci. 112, 4009–4014.